Photocatalysis

Enhanced Hydrogen Production from DNA-Assembled Z-Scheme TiO₂–CdS Photocatalyst Systems**

Ke Ma, Omer Yehezkeli, Dylan W. Domaille, Hans H. Funke, and Jennifer N. Cha*

Abstract: A wide range of inorganic nanostructures have been used as photocatalysts for generating H₂. To increase activity, Z-scheme photocatalytic systems have been implemented that use multiple types of photoactive materials and electron mediators. Optimal catalysis has previously been obtained by interfacing different materials through aggregation or epitaxial nucleation, all of which lowers the accessible active surface area. DNA has now been used as a structure-directing agent to organize TiO₂ and CdS nanocrystals. A significant increase in H₂ production compared to CdS or TiO₂ alone was thus observed directly in solution with no sacrificial donors or applied bias. The inclusion of benzoquinone (BQ) equidistant between the TiO₂ and CdS through DNA assembly further increased H₂ production. While the use of a second quinone in conjunction with BQ showed no more improvement, its location within the Z-scheme was found to strongly influence catalysis.

With increasing demands for alternative sources of fuel, extensive research has focused on discovering methods to generate renewable energy from earth-abundant resources. In recent years, a wide range of inorganic nanostructures with high surface areas and tunable band gaps have been synthesized and used as photocatalysts for splitting water into hydrogen and oxygen.[1–23] To increase their activity, Z-scheme photocatalytic systems have been implemented in which multiple types of photoactive materials simultaneously oxidize water and reduce molecules upon photoillumination.[1–12] In some cases, redox molecules or electron mediators have also been used to aid in electron shuttling between the different catalysts, facilitate charge separation, and inhibit recombination events. For example, Sasaki et al. recently showed that by mixing Ru/SrTiO₃:Rh with BiVO₄ and inducing aggregation through pH changes that higher amounts of H₂ and O₂ could be produced than either material alone.[1] In later work, they showed that adding [Co(bpy)₃]²⁺/ [Co(bpy)₃]³⁺ as redox mediators further enhanced water splitting performance.[2] Abe et al. reported similar work in which IO₃⁻/I⁻ was utilized to shuttle electrons between TiO₂ rutile and Pt-loaded TiO₂ anatase to produce H₂ under UV light.[3] To achieve catalysis under visible light, Kato and co-workers used a Pt/SrTiO₃: Rh-BiVO₄ system with Fe³⁺/Fe²⁺ as redox mediators.[4] Recently, solid-state Z-scheme systems have also been synthesized in which control over the interface between the different materials was found to be critical for higher fuel production.[5,17–22] For example, Tada et al. developed an anisotropic CdS/Au/TiO₂ system in which all the components were spatially fixed with Au facilitating electron transfer.[5] Metals other than gold have also been tested, including Ag,[20] Cd,[18] Cu,[19] ITO,[20] and reduced graphene oxide.[21]

In almost all of these cases, optimal catalysis is typically obtained by interfacing different materials through aggregation (for example, electrostatic interactions[1]) or epitaxial nucleation of one material on top of another. These methods, however, tend to decrease the overall accessible catalytic surface area because of the limited control over spatial organization of the separate components. Furthermore, the scope of different materials that can be produced by direct chemical synthesis is limited. Finally, since electron transfer largely depends on diffusion, simply mixing electron mediators with different catalysts in solution requires a high concentration of redox molecules to avoid rate limitations but which can lead to undesired side oxidation/reduction reactions. To address these challenges, we utilize DNA in this work as a structure-directing agent[23–36] to spatially organize well-defined TiO₂ and Pt decorated CdS (Pt@CdS) nanocrystals. By using DNA as an assembler, a significant increase in H₂ production was observed upon photoillumination compared to Pt@CdS or TiO₂ alone directly in solution. Potential limitations in H₂ production caused by negatively charged DNA on the Pt@CdS nanoparticles was simply fixed by controlling the amount of DNA per CdS nanorod. DNA also allowed positioning of a single or series of electron mediators site-specifically in between the two catalysts.
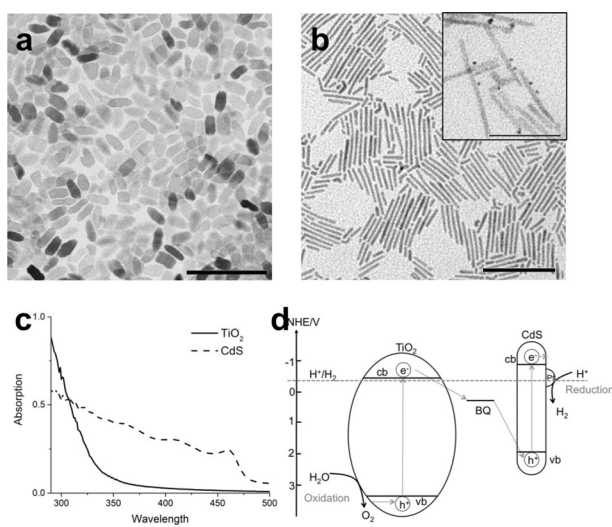
Well-defined Pt decorated CdS nanorods (NRs) and TiO₂ nanoparticles (NPs) were implemented as photocatalysts for the DNA-linked Z-scheme. Based on their respective energy levels, CdS or Pt@CdS should be able to efficiently reduce H⁺ to H₂ but TiO₂ cannot. TiO₂ NPs and CdS NRs were synthesized according to previous reports.[37,38] As shown in Figure 1a, the as-synthesized TiO₂ NPs possessed truncated rhombic shapes that were approximately 25 nm in length and 15 nm in diameter. The X-ray diffraction (XRD) analysis of

[*] K. Ma, Dr. O. Yehezkeli, Prof. D. W. Domaille, Prof. H. H. Funke, Prof. J. N. Cha
Department of Chemical and Biological Engineering
University of Colorado, Boulder, CO 80309-0596 (USA)
E-mail: Jennifer.Cha@colorado.edu

Prof. J. N. Cha
Materials Science and Engineering Program
University of Colorado (USA)

Figure 1. a) TEM image of TiO$_2$ nanocrystals with truncated rhombic shape. b) TEM image of CdS nanorods. Insert: Pt decorated CdS nanorods. c) UV/Vis spectrum of as-synthesized CdS nanorods and TiO$_2$ nanocrystals. d) Energy band diagram of the CdS–benzoquinone–TiO$_2$ system at pH 7. BQ = benzoquinone, cb = conduction band, vb = valence band. Scale bar: 100 nm.
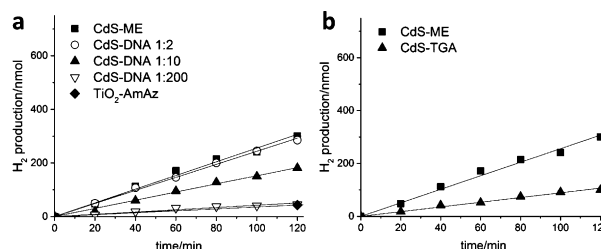
the TiO$_2$ particles (Supporting Information, Figure S1) showed them to have an anatase structure, and the UV/Vis measurements showed a strong absorption at about 350 nm (Figure 1c). As shown in Figure 1b, the CdS nanorods were about 6 nm in width and average 60 nm in length, which corresponded to an absorption onset of about 460 nm. Since the bandgap of the synthesized CdS NRs is about 2.7 eV, the rods should absorb all photon wavelengths less than 490 nm, while the TiO$_2$ bandgap of 3.83 eV causes it to absorb primarily in the UV range. The valence band and conduction band of the TiO$_2$ NPs were investigated by cyclic voltammetry (CV; Supporting Information, Figure S2).[39] As shown in Figure 1d, the conduction band of the TiO$_2$ NPs was determined to be −0.48 V vs. NHE, while the conduction band of the CdS NRs is −0.9 V vs. NHE.[36] At pH 7, the H$_2$ redox potential is −0.42 V vs NHE. Because the conduction band of the TiO$_2$ NPs is similar to the redox potential of H$_2$, it is difficult for TiO$_2$ to photoreduce protons, thereby making the TiO$_2$-CdS system an ideal platform for studying Z-scheme photocatalysis.

Next, to generate H$_2$ from the CdS NRs, Pt seeds were nucleated on the CdS through photodeposition.[40] TEM analysis showed that before and after platinum nucleation, the CdS nanocrystals retained their shape and size and that on average one Pt NP was bound per nanorod (Figure 1b). Next, ligand-exchange methods were developed to transfer the as-synthesized TiO$_2$ and CdS NPs into aqueous environments. After trying various small molecules, we found that the most successful way to transfer the TiO$_2$ NPs from toluene to water was to add a large excess of amine-(PEG)$_6$-azide. For the Pt@CdS NRs, we used our previously developed method of small-molecule ligand exchange by mercaptoethanol or thioglycolic acid.[41]

Once the TiO$_2$ and Pt@CdS NPs were transferred to the aqueous phase, DNA strands were conjugated to the NPs.

Previously developed methods were used to conjugate DNA strands to each Pt@CdS NR.[41] For the TiO$_2$ NPs, click chemistry was implemented to form covalent bonds between the azide groups on the TiO$_2$ and alkyne-terminated DNA (Supporting Information, Figure S3).[42] To qualitatively characterize DNA attachment, we reacted the DNA-TiO$_2$ with gold nanoparticles bound with complementary DNA. The AuNPs clearly associated with the TiO$_2$ NPs through DNA hybridization (Supporting Information, Figure S4). The use of copper catalysts to conjugate the DNA to the TiO$_2$ did not appear to affect the morphology or the absorption of the TiO$_2$ NPs (Supporting Information, Figure S5).

Once the DNA strands were conjugated to both catalysts, we probed their ability to produce H$_2$ at specific catalyst concentrations and compared these results to the azide-conjugated TiO$_2$ and ME-Pt@CdS. First, the azide-terminated TiO$_2$ NPs as expected showed almost no H$_2$ production (Figure 2a). In contrast, 43 nM mercaptoethanol coated Pt@CdS NRs (ME-Pt@CdS) produced about 230 nmol of
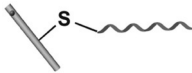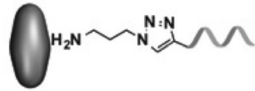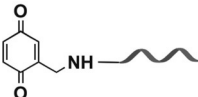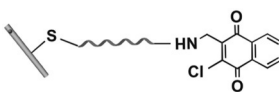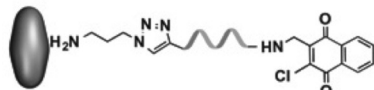

Figure 2. a) H$_2$ production from Pt@CdS NRs conjugated with different amounts of DNA (molar ratio of CdS/DNA = 1:2, 1:10, 1:200), and amine-(PEG)$_4$-azide coated TiO$_2$. Using molar ratios of CdS:DNA of 1:2 and 1:200 produced NRs attached with ca. 1.92 and ca. 189 DNA oligonucleotides, respectively, as determined by UV/Vis measurements. b) H$_2$ production from Pt@CdS NRs with mercaptoethanol (ME) (■) and thioglycolic acid (TGA) (▲).

H$_2$. Next, we measured H$_2$ production from the Pt@CdS NRs conjugated with about 200 DNA strands per particle. As shown in Figure 2a, having a large number of DNA strands attached caused a significant decrease in H$_2$ production as compared to the ME-Pt@CdS NRs. To determine if this effect was due to the presence of negatively charged groups at the photocatalyst surface, we also measured the amount of H$_2$ produced from Pt@CdS NRs conjugated with thioglycolic acid (TGA). As shown in Figure 2b, a substantial decrease in H$_2$ production was also observed from the negatively charged TGA-Pt@CdS as compared to the ME-Pt@CdS, indicating that the decrease in H$_2$ production could be caused by the high negative charge of TGA or DNA. It is also possible in the case of DNA that a high coverage of oligonucleotides covering a particle surface could also hinder proton adsorption. However, decreasing the amount of DNA attached to the Pt@CdS NRs to about 2–5 oligonucleotides per particle led to an improvement in H$_2$ production (Figure 2a) that gave results comparable to the ME-Pt@CdS NRs.

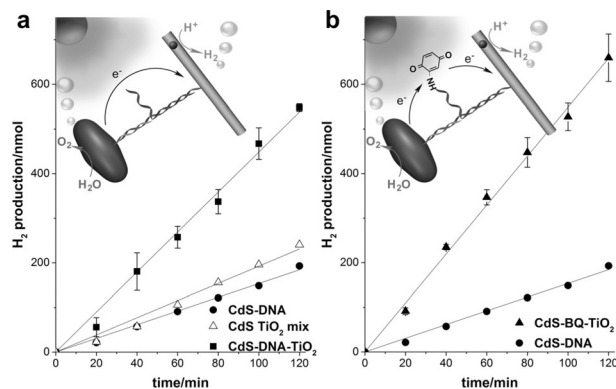To assemble the TiO$_2$-Pt@CdS clusters through DNA interactions, the thiolated DNA (DNA-1) on the Pt@CdS was designed to contain two domains, one of which is comple-

Table 1: DNA design and sequence.

DNA name	DNA usage	DNA sequence
DNA 1		thiol-CATTACGGCTTTCCCTATTA
DNA 2		alkyne-TAATAGGGAA
DNA 3		amine-TTTTTTAGCCGTAATG
DNA 4		thiol-CATTACGGCTTTCCCTATTATTTTTT-amine
DNA 5		alkyne-TAATAGGGAA-amine

mentary to the DNA (DNA-2) on the TiO_2, with the other complementary to a third amine-terminated strand (DNA-3; Table 1). DNA-3 was used later to place electron mediators such as benzoquinone site-specifically in between the TiO_2 and Pt@CdS. The DNA strands bridging the two photocatalysts were also designed to be 20 bases in length with a circa 40% G/C composition as this would yield good thermal stability in 100 mM NaCl and separate all the different components by 3–6 nm. After conjugating the DNA strands to the TiO_2 and Pt@Cds using nanoparticle/DNA molar ratios of 1:5 and 1:2, respectively, thermal annealing was used to generate the TiO_2-Pt@CdS clusters. TEM analysis of the DNA assembled catalysts showed the TiO_2 and Pt@CdS nanoparticles to be well associated with each other with no large aggregates forming (Supporting Information, Figure S6).

Dynamic light scattering measurements also showed an average cluster size of about 247 nm (Supporting Information, Figure S7). Next, the TiO_2-Pt@CdS clusters were tested for H_2 production. After photoirradiation under 1 sun for 2 h, the DNA assembled TiO_2-Pt@CdS nanoparticle clusters (Figure 3a) produced a significantly higher amount of H_2 than the TiO_2 or Pt@CdS NRs alone, with an overall gain of about 2.8 over Pt@CdS NR alone. Oxygen generated from the DNA linked Pt@CdS-TiO_2 was also determined and showed approximately a 2:1 H_2/O_2 ratio as determined by GC (Supporting Information, Figure S8). It should also be noted that the catalyst amount used in this work (ca. 0.1 mg) was significantly less than that used in other reports.[1,15,16] To test the importance of DNA assembly, H_2 production was measured from equimolar mixtures of mercaptoethanol-conjugated Pt@CdS NRs and amine-PEG-azide-coated TiO_2 NPs. In contrast to the DNA-assembled TiO_2-Pt@CdS catalysts, a dispersed solution of the two photocatalysts showed no improvement over Pt@CdS itself (Figure 3a), illustrating that any H_2 production enhancement was due solely to the DNA interaction. Furthermore, TEM analysis showed the DNA-linked TiO_2-Pt@CdS assemblies also

Figure 3. a) H_2 production from DNA-conjugated Pt@CdS (●), DNA-linked TiO_2-Pt@CdS (■), and simple mixtures of unlinked Pt@CdS and TiO_2 (△). b) H_2 production from DNA-conjugated Pt@CdS (●) and from DNA-linked Pt@CdS–benzoquinone–TiO_2 system (▲).

proved to be stable during photoillumination (Supporting Information, Figure S9).

The next hypothesis tested was that placement of electron mediators specifically between the two photocatalysts would enhance H_2 production further by inhibiting back reactivity to facilitate charge separation. Benzoquinone (BQ) was chosen as a candidate because its reduction potential of 0.283 V vs. NHE at pH 7 lies between the conduction band (CB) of TiO_2 NP and the valence band (VB) of CdS NR. BQ was attached to DNA-3 strands through a Michael addition.[43,44] Mass spectrometric analysis confirmed the successful conjugation of BQ to the DNA-3 strand (Supporting Information, Figure S10). Cyclic voltammetry (CV) studies revealed that amine functionalization of BQ altered its reduction potential to circa 0.073 V vs NHE at pH 7 (Supporting Information, Figure S11), which is still in between the CB and VB of TiO_2 and CdS, respectively. We next hybridized equimolar amounts of the DNA-1-Pt@CdS, DNA-2-TiO_2, and the DNA-3-BQ to make 43 nM concentrations of the Pt@CdS-BQ-TiO_2 and H_2 production was measured. As shown in Figure 3b, intercalat-

ing benzoquinone between the Pt@CdS and TiO$_2$ caused a further increase in H$_2$ production, with an overall 3.4-fold gain as compared to Pt@CdS itself and a 1.2-fold gain over the TiO$_2$-Pt@CdS assemblies without BQ. It should also be noted that this process required a very low concentration (nM) of electron mediator. As a comparison, previously reported examples of non-assembled catalysts in solution required millimolar concentrations of redox mediators,[2] which can lead to deleterious effects such as competing oxidation–reduction reactions. Furthermore, when nanomolar concentrations of BQ were simply mixed with either the DNA assembled TiO$_2$-Pt@CdS clusters or the Pt@CdS alone, no H$_2$ was produced due to BQ being competitively photoreduced in place of protons (Supporting Information, Figure S12). The solar-to-hydrogen (STH) energy conversion efficiency was also calculated. With 0.1 mg of Pt@CdS in solution, the STH values increased from 0.011 % with Pt@CdS to 0.031 % with TiO$_2$-Pt@CdS to 0.037 % with the TiO$_2$-BQ-Pt@CdS under one sun illumination at 97 mW cm^{-2}.
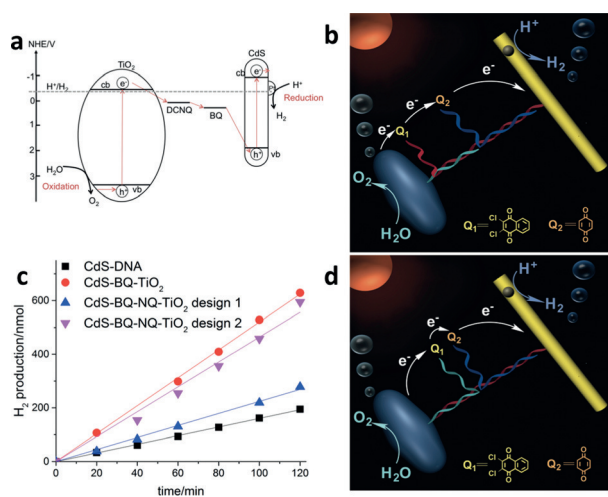
Apart from utilizing a single electron mediator, the incorporation of a second mediator was tested. For this, 2,3-dichloro-1,4-napthoquinone (DCNQ) was used, as its reduction potential of −0.077 V vs NHE is more positive than the CB of TiO$_2$ but more negative than the redox potential of BQ. In this case, the excited electrons are expected to travel from TiO$_2$ to DCNQ to BQ to Pt@CdS (Figure 4a). To achieve this, the DNA-1 strand was modified to include a thiol group at its 5′ end and an amine at the 3′ end (DNA-4), to place the DCNQ in close proximity to the TiO$_2$ NP (Figure 4b).[45] In testing the TiO$_2$-DCNQ-BQ-Pt@CdS clusters however for catalysis, we found that less H$_2$ was produced than the Pt@CdS-BQ-TiO$_2$ system (Figure 4c). Although an additional redox mediator may facilitate the electron transfer, it is also possible that two intermediates may slow down the kinetics of the process owing to the additional redox step.

Because chronoamperometry studies however shown that the electron-transfer rates of BQ and DCNQ do not differ significantly from each other (Supporting Information, Figure S13), another more likely scenario is that the close proximity of the DCNQ to the TiO$_2$ leads to back reactivity, preventing electron mobility from DCNQ to BQ. To investigate this further, we modified DNA-2 to possess an alkyne at its 3′ end and an amine at its 5′ end (DNA-5; Table 1). This design would cause the DCNQ to be separated from the TiO$_2$ surface by about 3 nm but be immediately next to the BQ (Figure 4d). The TiO$_2$-DNA-5-DCNQ were next hybridized with the DNA-1-Pt@CdS and DNA-3-BQ and tested for H$_2$ production. As shown in Figure 4c, while increasing the distance between the DCNQ and TiO$_2$ did increase the H$_2$ production from the first design of TiO$_2$-DCNQ-BQ-Pt@CdS system (with DNA-4), the overall H$_2$ yield was comparable to the TiO$_2$-BQ-Pt@CdS but not higher. Because the two quinones have similar energy levels and a similar electron-transfer rate, the electron transfer might not significantly change from the Pt@CdS-BQ-TiO$_2$ system, or the electron may even be prevented from transferring to the Pt@CdS by undergoing cyclic oxidation/reduction processes between the DCNQ and BQ. To cause an improvement in photocatalysis and H$_2$ production then, alternate quinones, increasing the distance between the mediators or using dynamic hybridization events need to be investigated in future studies.

In conclusion, a method was demonstrated for self-assembling different photocatalysts and electron mediators using DNA interactions for enhanced H$_2$ production. DNA was used to construct a well-organized Z-scheme photocatalytic system that could produce H$_2$ directly in water under solar illumination. The DNA assembled Pt@CdS and TiO$_2$ clusters showed a significant improvement in H$_2$ production compared to either single photocatalysts or unassembled, dispersed catalyst mixtures. Using DNA also enabled us to site specifically place electron mediators in between the TiO$_2$ and CdS and we found that while the use of benzoquinone alone improved H$_2$ production, utilizing an additional mediator did not improve catalysis. These results demonstrate that to increase the production of H$_2$ even more, both the redox potentials and spatial positioning of all the different Z-scheme components need to further optimized, and this will be studied in future work.

Figure 4. a) Energy band diagram of the Pt@CdS-BQ-DCNQ-TiO$_2$ system. b) H$_2$ production from Pt@CdS-BQ-DCNQ-TiO$_2$ design 1 system. c) H$_2$ production from Pt@CdS-BQ-DCNQ-TiO$_2$ assemblies versus Pt@CdS-BQ-TiO$_2$ (●) or Pt@CdS-DNA alone (■) design 1 (▲) design 2 (▼). d) H$_2$ production from CdS-BQ-DCNQ-TiO$_2$ design 2 system.

[1] Y. Sasaki, H. Nemoto, K. Saito, A. Kudo, *J. Phys. Chem. C* **2009**, *113*, 17536–17542.

[2] Y. Sasaki, H. Kato, A. Kudo, *J. Am. Chem. Soc.* **2013**, *135*, 5441–5449.

[3] R. Abe, K. Sayama, K. Domen, H. Arakawa, *Chem. Phys. Lett.* **2001**, *344*, 339–344.

[4] H. Kato, M. Hori, R. Konta, Y. Shimodaira, A. Kudo, *Chem. Lett.* **2004**, *33*, 1348–1349.

[5] H. Tada, T. Mitsui, T. Kiyonaga, T. Akita, K. Tanaka, *Nat. Mater.* **2006**, *5*, 782–786.

[6] J. Yu, S. Wang, J. Low, W. Xiao, *Phys. Chem. Chem. Phys.* **2013**, *15*, 16883–16890.

[7] K. Maeda, *ACS Catal.* **2013**, *3*, 1486–1503.

[8] Y. Tachibana, L. Vayssieres, J. R. Durrant, *Nat. Photonics* **2012**, *6*, 511–518.

[9] H. Kato, Y. Sasaki, A. Iwase, A. Kudo, *Bull. Chem. Soc. Jpn.* **2007**, *80*, 2457–2464.

[10] S. S. K. Ma, K. Maeda, T. Hisatomi, M. Tabata, A. Kudo, K. Domen, *Chem. Eur. J.* **2013**, *19*, 7480–7486.

[11] T. Kothe, N. Plumeré, A. Badura, M. M. Nowaczyk, D. A. Guschin, M. Rogner, W. Schuhmann, *Angew. Chem. Int. Ed.* **2013**, *52*, 14233–14236; *Angew. Chem.* **2013**, *125*, 14483–14486.

[12] D. J. Martin, P. J. T. Reardon, S. J. A. Moniz, J. Tang, *J. Am. Chem. Soc.* **2014**, *136*, 12568–12571.

[13] G. Hitoki, T. Takata, J. N. Kondo, M. Hara, H. Kobayashi, K. Domen, *Chem. Commun.* **2002**, 1698–1699.

[14] R. Abe, T. Takata, H. Sugihara, K. Domen, *Chem. Commun.* **2005**, 3829–3831.

[15] K. Maeda, M. Higashi, D. Lu, R. Abe, K. Domen, *J. Am. Chem. Soc.* **2010**, *132*, 5858–5868.

[16] H. J. Yun, H. Lee, N. D. Kim, D. M. Lee, S. Yu, J. Yi, *ACS Nano* **2011**, *5*, 4084–4090.

[17] K. Sekizawa, K. Maeda, K. Domen, K. Koike, O. Ishitani, *J. Am. Chem. Soc.* **2013**, *135*, 4596–4599.

[18] X. Wang, G. Liu, L. Wang, Z. Chen, G. Q. Lu, H. M. Cheng, *Adv. Energy Mater.* **2012**, *2*, 42–46.

[19] S. Sato, T. Arai, T. Morikawa, K. Uemura, T. M. Suzuki, H. Tanaka, T. Kajino, *J. Am. Chem. Soc.* **2011**, *133*, 15240–15243.

[20] Z. Liu, Z. G. Zhao, M. Miyauchi, *J. Phys. Chem. C* **2009**, *113*, 17132–17137.

[21] A. Iwase, Y. H. Ng, Y. Ishiguro, A. Kudo, R. Amal, *J. Am. Chem. Soc.* **2011**, *133*, 11054–11057.

[22] P. Zhou, J. Yu, M. Jaroniec, *Adv. Mater.* **2014**, *26*, 4920–4935.

[23] C. Li, J. Yuan, B. Han, L. Jiang, W. Shangguan, *Int. J. Hydrogen Energy* **2010**, *35*, 7073–7079.

[24] X. Liu, A. Niazov-Elkan, F. Wang, I. Willner, *Nano Lett.* **2013**, *13*, 219–225.

[25] D.-K. Lim, K.-S. Jeon, H. M. Kim, J-M. Nam, Y. D. Suh, *Nat. Mater.* **2010**, *9*, 60–67.

[26] W. Yan, L. Xu, C. Xu, W. Ma, H. Kuang, L. Wang, N. A. Kotov, *J. Am. Chem. Soc.* **2012**, *134*, 15114–15121.

[27] L. Xu, H. Kuang, C. Xu, W. Ma, L. Wang, N. A. Kotov, *J. Am. Chem. Soc.* **2012**, *134*, 1699–1709.

[28] R. Schreiber, J. Do, E.-M. Roller, T. Zhang, V. J. Schuller, P. C. Cickels, J. Feldmann, T. Liedl, *Nat. Nanotechnol.* **2014**, *9*, 74–76.

[29] G. P. Acuna, M. Bucher, I. H. Stein, C. Steinhauer, A. Kuzyk, P. Holzmeister, R. Schreiber, A. Moroz, F. D. Stefani, T. Liedl, F. C. Simmel, P. Tinnefeld, *ACS Nano* **2012**, *6*, 3189–3195.

[30] H. Yan, S. H. Park, G. Finkelstein, J. H. Reif, *Science* **2003**, *301*, 1882–1884.

[31] J. Sharma, Y. Ke, C. Lin, R. Chhabra, Q. Wang, J. Nangreave, Y. Liu, H. Yan, *Angew. Chem. Int. Ed.* **2008**, *47*, 5157–5159; *Angew. Chem.* **2008**, *120*, 5235–5237.

[32] J. Liu, Y. Lu, *J. Am. Chem. Soc.* **2003**, *125*, 6642–6643.

[33] R. Tel-Vered, O. Yehezkeli, H. B. Yildiz, O. I. Wilner, I. Willner, *Angew. Chem. Int. Ed.* **2008**, *47*, 8272–8276; *Angew. Chem.* **2008**, *120*, 8396–8400.

[34] W. Sun, E. Boulais, Y. Hakobyan, W. L. Wang, A. Guan, M. Bathe, P. Yin, *Science* **2014**, *346*, 1258361.

[35] H. T. Maune, S.-p. Han, R. D. Barish, M. Bockrath, W. A. Goddard III, P. W. K. Rothemund, E. Winfree, *Nat. Nanotechnol.* **2010**, *5*, 61–66.

[36] R. Gill, F. Patolsky, E. Katz, I. Willner, *Angew. Chem. Int. Ed.* **2005**, *44*, 4554–4557; *Angew. Chem.* **2005**, *117*, 4630–4633.

[37] C.-T. Dinh, T.-D. Nguyen, F. Kleitz, T.-O. Do, *ACS Nano* **2009**, *3*, 3737–3743.

[38] R. D. Robinson, B. Sadtler, D. O. Demchenko, C. K. Erdonmez, L.-W. Wang, A. P. Alivisatos, *Science* **2007**, *317*, 355–358.

[39] S. K. Haram, B. M. Quinn, A. J. Bard, *J. Am. Chem. Soc.* **2001**, *123*, 8860–8861.

[40] G. Dukovic, M. G. Merkle, J. H. Nelson, S. M. Hughes, A. P. Alivisatos, *Adv. Mater.* **2008**, *20*, 4306–4311.

[41] H. Noh, S. M. Goodman, P. Mohan, A. P. Goodwin, P. Nagpal, J. N. Cha, *RSC Adv.* **2014**, *4*, 8064.

[42] V. Hong, S. I. Presolki, C. Ma, M. G. Finn, *Angew. Chem. Int. Ed.* **2009**, *48*, 9879–9883; *Angew. Chem.* **2009**, *121*, 10063–10067.

[43] J. S. Yadav, B. V. S. Reddy, T. Swamy, K. S. Shankar, *Monatsh. Chem.* **2008**, *139*, 1317–1320.

[44] E. Katz, H.-L. Schmidt, *J. Electroanal. Chem.* **1993**, *360*, 337–342.

[45] V. K. Tandon, H. K. Maurya, *Tetrahedron Lett.* **2009**, *50*, 5896–5902.